

## Full paper

## Moisture induced electricity for self-powered microrobots



Yang Wang <sup>a,1</sup>, Ming Dai <sup>b,1</sup>, Heting Wu <sup>a,c</sup>, Lin Xu <sup>a,e</sup>, Tongtong Zhang <sup>a,c</sup>, Wenshuai Chen <sup>b,\*</sup>, Zhong Lin Wang <sup>a,d,\*\*</sup>, Ya Yang <sup>a,c,e,\*\*\*</sup>

<sup>a</sup> CAS Center for Excellence in Nanoscience, Beijing Key Laboratory of Micro-Nano Energy and Sensor, Beijing Institute of Nanoenergy and Nanosystems, Chinese Academy of Sciences, Beijing 101400, PR China

<sup>b</sup> Key Laboratory of Bio-based Material Science and Technology, Ministry of Education, Northeast Forestry University, Harbin 150040, PR China

<sup>c</sup> School of Nanoscience and Technology, University of Chinese Academy of Sciences, Beijing 100049, PR China

<sup>d</sup> School of Material Science and Engineering, Georgia Institute of Technology, Atlanta, GA 30332-0245, USA

<sup>e</sup> Center on Nanoenergy Research, School of Physical Science and Technology, Guangxi University, Nanning 530004, PR China

## ARTICLE INFO

## Keywords:

Water harvesting  
Self-powered microrobots  
Insect-scale robots  
Hygroscopic gel

## ABSTRACT

Sustainable operation of microrobots mandatorily needs a continuous supply of energy, which is usually provided by a battery. However, with the miniaturization of the microrobot, the reduction of weight, and the limited lifetime of battery, self-powering of microrobot is a key challenge. Inspired by the crawling of cockroaches, we present an untethered insect-scale robot driven by moisture induced electric power. A moisture-based energy harvesting device has been exploited and embedded in the microrobot, which can capture and store atmospheric water under various environmental conditions through a hygroscopic gel and generate electricity based on redox reaction. The device produces an output voltage of ~1.4 V and an output current of ~43 mA. A combination of moisture-electricity powered vertical vibration and the asymmetric structural design of the microrobot enables its forward locomotion at an average speed of ~4.01 cm/s. Our work could facilitate multifunctionality in future self-powered microrobots and mesoscale devices.

## 1. Introduction

Microrobots can perform tasks, such as confined space exploration and actuation with multiple degrees of freedom, which are difficult to achieve with conventional robots [1–7]. However, providing sufficient power for sustainable operation of microrobots is challenging. Lithium-ion batteries (LIBs) are the main power source for conventional robots [8,9]. However, the LIBs have limited structure and specific energies, and will create an extra load and some increased volume for the microrobots, restricting the multifunctionality for future microrobot development [10,11].

There is growing interest in insect-scale (micro-scale) robots that do not need LIBs and have effective and complex mobility, such as robotic flies [12], strider-like robots [13,14] and soft robots [15–18]. These robots, however, usually need an external stimulus, such as light, heat, humidity, or magnetism, as an actuation source to realize sufficient mobility, leading to instability under environmental effects [19–23]. To

address these issues, our group developed a floating robotic insect that can harvest energy from water [24]. However, the demand for a water source restricts its activity. Thus, harvesting energy from ambient humidity is an expectant route that can provide portable and clean energy for microrobots [25–30], because moisture can be freely obtained anywhere on earth.

Some pioneering studies have explored various advanced materials and techniques for enhancing the capability of atmospheric water capture [31–41] and moisture-based electricity generation [42–46]. For example, polypyrrole chloride/poly N-isopropylacrylamide moisture absorbing gel exhibits a daily water harvest of 19.2 L/kg of the corresponding xerogel at a relative humidity (RH) of 60% [47]. A hybrid photocatalysis system that comprises a hygroscopic hydrogel and cupric oxide and barium titanate nanoparticles can split 36.5 mg of absorbed atmospheric water to produce a photocurrent of 224.3  $\mu\text{A}/\text{cm}^2$  [48]. Protein nanowires (NWs) were employed to produce a voltage of ~0.5 V and a current of ~110 nA under a load of 2 M $\Omega$  from ambient humidity

\* Corresponding author.

\*\* Corresponding authors at: CAS Center for Excellence in Nanoscience, Beijing Key Laboratory of Micro-Nano Energy and Sensor, Beijing Institute of Nanoenergy and Nanosystems, Chinese Academy of Sciences, Beijing 101400, PR China

E-mail addresses: [chenwenshuai@nefu.edu.cn](mailto:chenwenshuai@nefu.edu.cn) (W. Chen), [zhong.wang@mse.gatech.edu](mailto:zhong.wang@mse.gatech.edu) (Z.L. Wang), [yang@binn.cas.cn](mailto:yang@binn.cas.cn) (Y. Yang).

<sup>1</sup> Y. Wang and M. Dai contributed equally to this work.

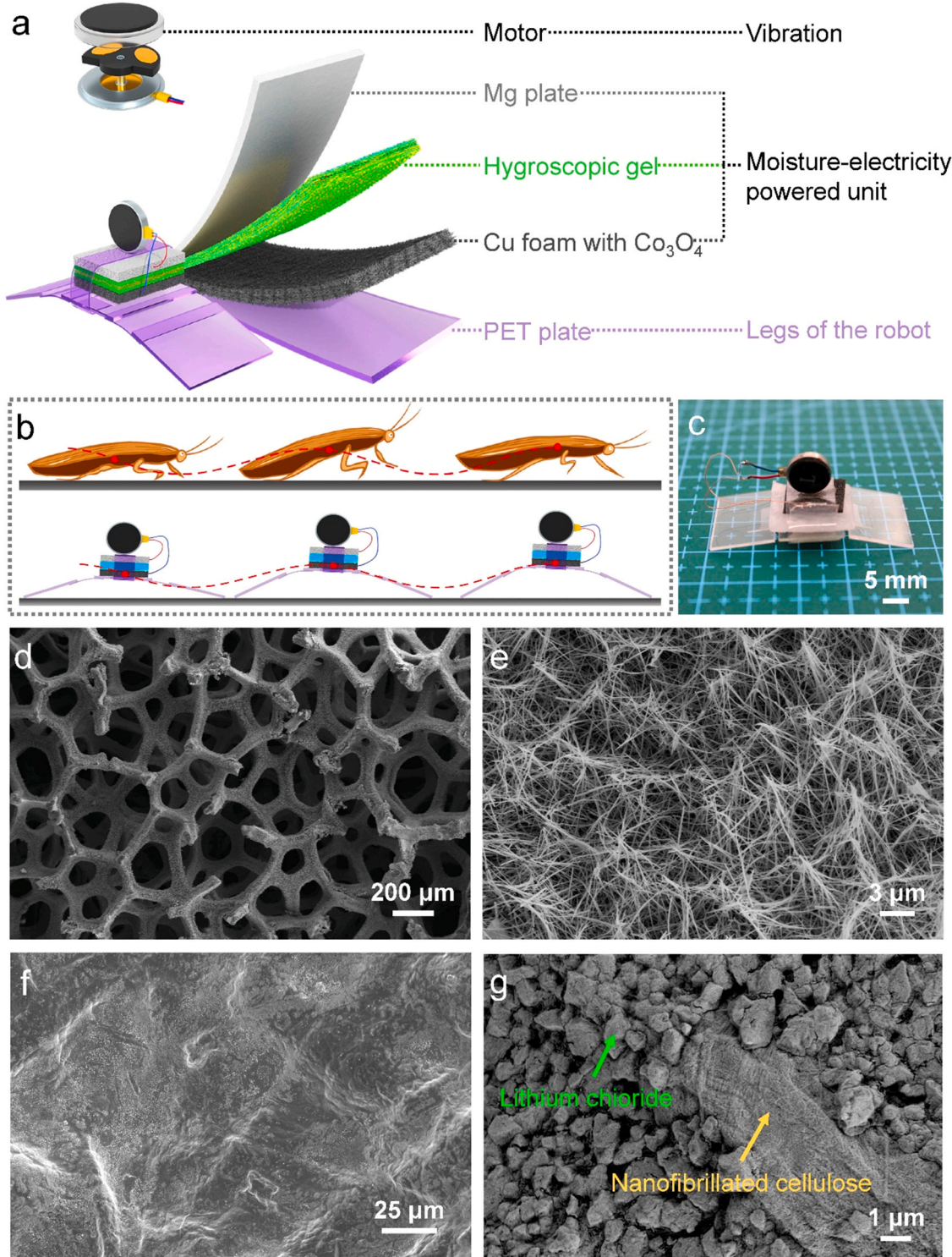


**Fig. 1.** Robot design, assembly, and working mechanism. (a) Schematics of the microrobot with moisture-electricity powered unit. (b) Comparison of the center of mass path for a cockroach and that for our robot. (c) Photograph of the assembled robot. (d) SEM image of Cu foam. e  $\text{Co}_3\text{O}_4$  nanowires coated on Cu foam. (f, g) SEM images of the surface of hygroscopic gel.

[49]. Bulk graphene oxide was used to exploit a hydroelectric generator unit to produce electricity from air with an output voltage of  $\sim 1.5$  V. These studies stimulated the construction of self-propulsion systems [50]. However, existing atmospheric water capturing and moisture-based energy harvesting technologies have not yet demonstrated powerful ability to drive soft actuators and electric motors. New strategies for insect-scale robots should be developed along with the

introduction of moisture-based energy harvesting devices.

Here, we present a cockroach crawling-inspired microrobot powered by moisture induced electric power. The intrinsic structural design enables the integration of multiple functions into a microrobot: moisture capture, energy harvesting, and actuation. The robot contains a moisture-based generator that can acquire water from ambient air through a hygroscopic gel. The absorbed water is used for electricity

generation to drive a micromotor via redox reactions. The micromotor transmits mechanical vibration to the asymmetric folding body of the robot, allowing the robot to rapidly move forward. The microrobot exhibits a power density of approximating  $8.5 \text{ mW/cm}^2$  and an average forward movement speed of  $4.01 \text{ cm/s}$ .

## 2. Experimental section

### 2.1. Preparation of hygroscopic gel

NFC was individualized from poplar wood powder and its preparation was referred to the previous work [56]. 20 g of 1 wt% NFC aqueous suspension was added into a 150-mL beaker. Then, 40 g of 5 wt% LiCl aqueous solution was slowly added to the NFC suspension along the beaker wall. The beaker was kept at room temperature for 12 h, which led to the generation of an NFC/LiCl composite hydrogel. Excess LiCl solution in the beaker was sucked out and the hydrogel was put into a freezer for 12 h. Lyophilization was subsequently conducted using a freeze-drier to yield hygroscopic gel.

### 2.2. Moisture absorption using the hygroscopic gel

The absorption of water vapor from air using the hygroscopic gel was carried out for 12 h in a constant-temperature and -humidity chamber (GDJS-225, Beijing Yashilin Testing Equipment Co. Ltd., China) at  $26^\circ\text{C}$  and various RH values and at 50% RH and various temperatures. The moisture absorption of the gel was also evaluated in a normal room, in which the temperature and humidity slightly fluctuated, for 12 h. The water uptake of the gel after moisture absorption was calculated as:

$$\text{Water uptake} = (m_w - m_d)/m_d \quad (1)$$

where  $m_w$  denotes the mass of the wet gel after moisture absorption at a given time and  $m_d$  is the mass of the dry gel before the absorption of water vapor from air.

### 2.3. Storage of the moisture-absorbed gel at various environment

The wet gel that had absorbed plenty of moisture was placed in environments with a moderate RH of 40% and a moderate temperature of  $25^\circ\text{C}$ , a high RH of 80% and a moderate temperature of  $25^\circ\text{C}$ , a moderate RH of 40% and a high temperature of  $40^\circ\text{C}$ , a high RH of 80% and a high temperature of  $40^\circ\text{C}$ , room RH and room temperature, and outdoor RH and outdoor temperature on a normal winter day in Harbin City, in sequence. The mass of the gel was recorded once per hour. After 12 h in the given environment, the gel was taken out and put into a hermetic desiccator and stored at room temperature for 12 h. Then, the gel was placed in the next environment for 12 h.

### 2.4. Fabrication of $\text{Co}_3\text{O}_4$ nanowires

Copper foam (thickness: 3 mm) was cut into plates ( $10 \text{ mm} \times 10 \text{ mm}$ ) and cleaned with acetone, ethanol, and deionized water, in sequence, for 10 min, respectively. The prepared copper foam plates were immersed in an aqueous solution (50 mL) of 1 M  $\text{Co}(\text{NO}_3)_2$  and 5 M  $\text{Co}(\text{NH}_2)_2$ . Next, the solution was put into a Teflon-lined stainless-steel autoclave, which was placed in an oven at  $90^\circ\text{C}$  for 6 h. The prepared foam plates were rinsed with deionized water and then annealed in air at  $250^\circ\text{C}$  for 60 min.

### 2.5. Fabrication of the microrobot

Three acrylic plates ( $10 \text{ mm} \times 15 \text{ mm} \times 0.25 \text{ mm}$ ) were used as the crossbeam and two legs of the robot. Two flexible acrylic films ( $5 \text{ mm} \times 15 \text{ mm} \times 0.1 \text{ mm}$ ) were used to connect the crossbeam and legs via UV-cured glue. During the assembling process, the highest point

of the hind leg is higher than the highest point of the foreleg. The prepared copper foam was fixed on the crossbeam of the robot via double-sided tape. A magnesium plate was fixed on a flexible belt connected to the crossbeam. Then, the hygroscopic gel was sandwiched between the copper foam and magnesium plate. Finally, an electric motor was attached on the top center of the robot and connected to the copper foam and magnesium plate through copper wires.

### 2.6. Characterization and measurements

The morphology and structure of the hygroscopic gel and copper foam were investigated using field-emission scanning electron microscopy (Sigma 500, Zeiss, Germany; Apreo S, FEI, USA). The 3D microstructure of the gel was acquired using X-ray 3D microscopy (nanoVoxel-3000, Sanying Precision Instruments Co., Ltd., China) by transmitting X-rays through the gel with a rotation step of  $0.25^\circ$  and a pixel size of  $0.5 \mu\text{m}$ . Wetting analysis was conducted using a contact angle meter (DSA100, KRUSS, Germany). The output voltage and current of the device were measured using a digital source meter (Keithley, 2611B). The robot COM was tracked by a high-speed camera (Qianyanlang, 2F04).

## 3. Results and discussion

A prototype  $3.2 \text{ cm} \times 1 \text{ cm}$  robot with folding body design was assembled. Its motion is driven by transforming moisture-electricity powered mechanical vibration to the asymmetric folding body of the robot (Fig. 1a and c). We used a rigid polyethylene terephthalate (PET) plate (thickness: 0.25 mm) as the crossbeam and legs of the robot, and flexible PET film (thickness: 0.1 mm) as the hinge springs. To make the robot body asymmetric, the highest point of the foreleg is lower than the highest point of the hind leg. The moisture-based electricity generation unit, which comprises layers of a copper (Cu) foam, a hygroscopic gel, and a magnesium (Mg) sheet, is attached on the PET crossbeam. A small electric motor, used as the vibration unit, is installed at the top center of the robot. The body of the robot resembles an origami pattern. It undergoes periodic extension and contraction, created by the moisture-electricity powered vibration motor, to generate a forward force to drive the robot. The trajectory of the robot's center of mass (COM) is very similar to that of a crawling cockroach, as illustrated in Fig. 1b [51]. Unlike robots driven by the piezoelectric effect under a high alternating-current driving voltage, our design uses a universal motor under a low direct-current voltage, avoiding the requirement for external power sources (Movie S1) [52].

Supplementary material related to this article can be found online at doi:10.1016/j.nanoen.2021.106499.

Our robot's energy generation mechanism is modeled after metal-air batteries (MABs). Cobalttisic oxide ( $\text{Co}_3\text{O}_4$ ) deposited on Cu foam serves as the cathode and an Mg sheet serves as the anode. A low-magnification scanning electron microscopy (SEM) image shows the porous structure of the Cu foam (Fig. 1d).  $\text{Co}_3\text{O}_4$  nanowires freely stand on the foam substrate, forming a three-dimensional (3D) hierarchical structure (Fig. 1e). The average length of the  $\text{Co}_3\text{O}_4$  nanowires is approximately  $8 \mu\text{m}$  along the growth direction. The Raman spectra confirms the chemical composition of the  $\text{Co}_3\text{O}_4$  nanowires (Fig. S1). A hygroscopic gel, which absorbs moisture from the ambient environment, is placed between the two electrodes. The gel was produced by exchanging a wood-derived nanofibrillated cellulose (NFC) aqueous suspension (Fig. S2) with lithium chloride (LiCl) aqueous solution, followed by lyophilization. The gel has a porous structure with hygroscopic LiCl microparticles that interpenetrate into the hydrophilic, high-aspect-ratio, and entangled NFC networks (Fig. 1f and g). The as-assembled energy generation device shares many of the advantages of MABs, including low material cost, high energy density, and harmlessness. Unlike conventional MABs that require a liquid electrolyte, our device uses a solid hygroscopic gel, which can combine with the robot, capture

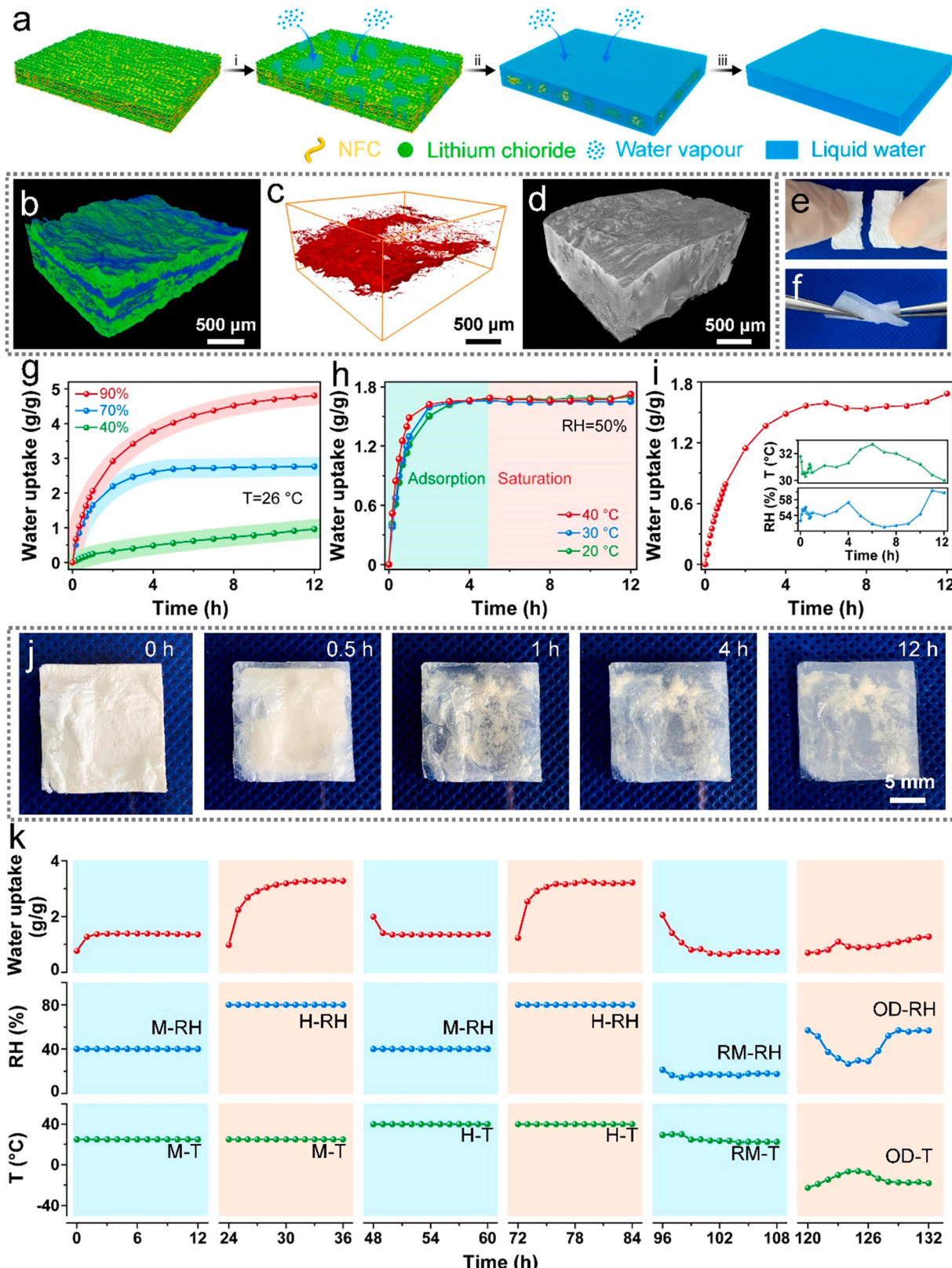


**Fig. 2.** Absorption of moisture from air using hygroscopic gel. (a) Schematic of the moisture absorption process of the gel. (b) X-ray 3D microscopy image of the gel. (c) 3D image of spatial pore distribution of the gel. (d) X-ray 3D microscopy image of the gel after it absorbed plenty of moisture from air. Photographs of the gel (e) before and (f) after moisture absorption upon bending and twisting. The moisture absorption behavior of the gel at various (g) RH values and (h) temperatures and (i) in a normal room. Inset of (i) shows the corresponding RH value and temperature of the room at a given time. (j) Photographs of the gel at various moisture absorption times corresponding to (i). (k) The water grabbing ability of the gel when placing the moisture-absorbed gel in environments with a moderate RH (M-RH) and a moderate temperature (M-T), a high RH (H-RH) and a M-T, a M-RH and a high temperature (H-T), a H-RH and a H-T, room RH (RM-RH) and room temperature (RM-T), and outdoor RH (OD-RH) and outdoor temperature (OD-T) in winter, in sequence.

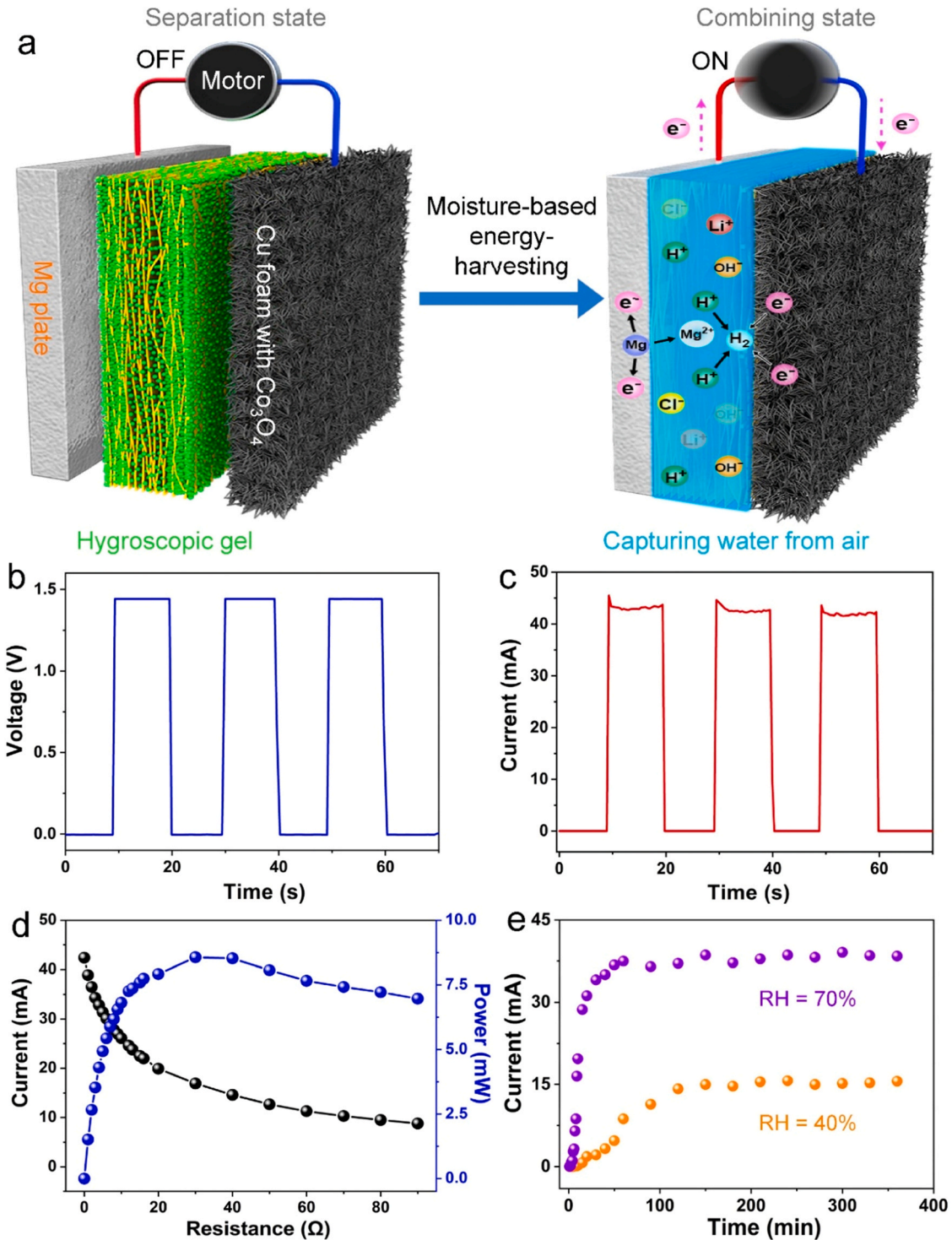


**Fig. 3.** Schematic and electric output characteristics of moisture-based energy harvesting device. (a) Illustration of electricity generation mechanism. Measured (b) output voltage and (c) current of the device. (d) Measured output current of the device under various load resistances and the corresponding output powers. (e) Current output under various RH conditions.

water from air for moisture-based energy generation, and adjust the corresponding electrical properties [53,54].

The critical step of moisture-based energy harvesting is the capture of atmospheric water. The moisture absorption process of the hydroscopic gel is schematically shown in Fig. 2a. When exposed to air, LiCl particles at the surface of the gel quickly absorb moisture. The absorbed water aggregates, liquefies, and gradually dissolves the LiCl. Because the surface of NFC contains a large number of hydroxyl groups, the porous

NFC aerogel is superhydrophilic (Fig. S3 and Movie S2), leading to rapid absorption and storage of the liquid water. The liquid water derived from LiCl-absorbed moisture is transported from the surface to the inner part of the gel through channels within the NFC networks. The moisture absorption continues until the gel saturates under the ambient conditions.

Supplementary material related to this article can be found online at doi:10.1016/j.nanoen.2021.106499.

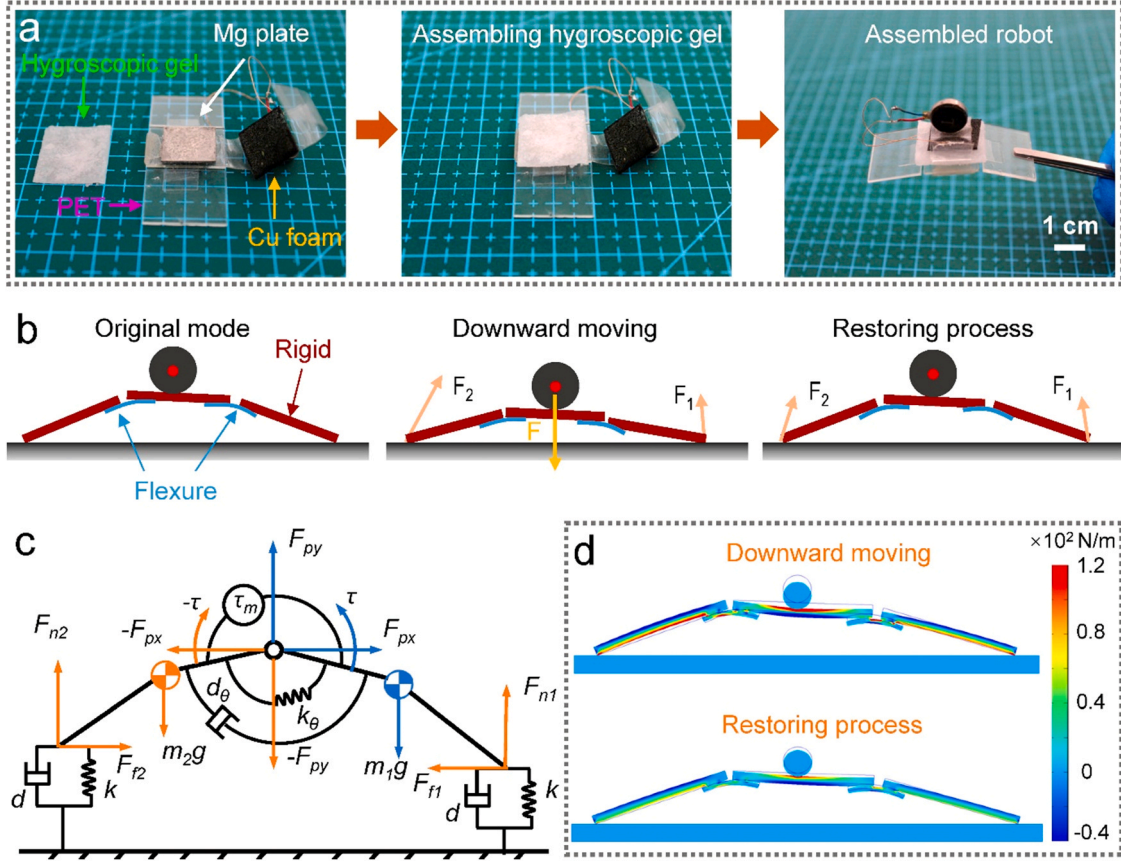


**Fig. 4.** Assembly of microrobot and locomotion analysis. (a) Photographs of assembly process. (b) Movement behavior of the microrobot. (c) Simplified dynamic model of microrobot based on a spring-damper system. (d) Simulation results on the actuated switch between two states.

The hygroscopic gel has a porous hierarchical structure. LiCl particles and NFC are densely packed at the surface but loosely packed in the inner region (Fig. 2b and Movie S3). The inner part of the gel contains pores with a size of several hundred microns (Fig. 2c), which contributes greatly to the large pore volume of the gel. In contrast, the pores on the gel periphery are very small. The intrinsic inhomogeneous nanofiber/particle interconnected porous structure is beneficial for moisture absorption, absorbed water vapor aggregation and liquification, water transportation, and storage. After a certain amount of moisture is absorbed, the LiCl particles are completely dissolved, and the wet gel swells (Fig. 2d, Movie S4, and Movie S5). The gel becomes flexible and can be repeatedly bent and twisted (Fig. 2f). In contrast, the dry gel is very brittle and breaks when bent (Fig. 2e).

Supplementary material related to this article can be found online at doi:10.1016/j.nanoen.2021.106499.

The absorption of water vapor from air was measured at various RH values and temperatures to evaluate the atmospheric water absorption capacity of the gel. The absorption rate and water uptake increased with increasing ambient humidity (Fig. 2g). At 90% RH and 26 °C, 0.1676 g of gel can absorb 0.8061 g of water vapor from air in 12 h (i.e., the gel can absorb 4.81 times its own weight of moisture). At 50% RH, when the temperature was increased from 20 °C to 40 °C, the absorption rate of the gel increased slightly, and the gel became saturated after ~5 h (Fig. 2h). In a normal room, where the temperature and humidity fluctuated, the gel still quickly absorbed moisture with water uptake of 1.68 g g<sup>-1</sup> in 12 h (Fig. 2i). During absorption, the gel became gradually wetted from the peripheral region to the inner region (Fig. 2j, Fig. S5, S6 and S7). The absorbed water was stored within the superhydrophilic nanofiber networks, making the wet gel translucent. The moisture-absorbed gel was placed in environments with a moderate RH (M-RH) of 40% and moderate temperature (M-T) of 25 °C, high RH (H-

RH) of 80% and M-T of 25 °C, M-RH of 40% and high temperature (H-T) of 40 °C, H-RH of 80% and H-T of 40 °C, room RH (RM-RH) and room temperature (RM-T), and outdoor RH (OD-RH) and outdoor temperature (OD-T) in winter, in sequence. It quickly absorbed or released water to adapt the changes of the environment, and always contained a certain amount of water (Fig. 2k), indicating its universal applicability in various environments.

Fig. 3a shows a schematic representation of our moisture-based energy harvesting device. The Mg plate is acted as the anode and the Co<sub>3</sub>O<sub>4</sub> nanowires deposited on the Cu foam served as the cathode. As the water in the air are absorbed onto the hygroscopic gel and dissolve the LiCl, Li<sup>+</sup> and Cl<sup>-</sup> ions dissociate and disperse in the water. A reduction reaction occurs at the cathode ( $2H^+ + 2e^- \rightarrow H_2\uparrow$ ) and an oxidation reaction occurs at the anode ( $Mg - 2e^- \rightarrow Mg^{2+}$ ). These reactions drive electrons to flow through an external circuit and produce current, powering the micromotor that generates mechanical vibration. To evaluate the operational performance, we subjected the device to repeated cycling using an ON/OFF switch (Fig. S8). The device produced an output voltage of approximately 1.4 V and an output current of approximately 42.8 mA (Fig. 3b and c). The output current decreased and the output power increased as the load was increased from 1 to 100 Ω. A maximum power density of ~8.5 mW/cm<sup>2</sup> was achieved at an optimal resistance of ~30 Ω (Fig. 3d). The electric performance of the device outstanding enhanced with increasing the RH, showing its environmental humidity-dependent features (Fig. 3e). The output current gradually decreased due to the depletion of harvesting water and electrodes at initial 100 min, and then kept stable (Fig. S9).

For assembling the microrobot, the hygroscopic gel is sandwiched between the Cu foam and the Mg plate. The whole process is convenient and repeatable (Fig. 4a). The asymmetric folding body of the robot and the vertical vibration generate a forward force to drive the robot moving

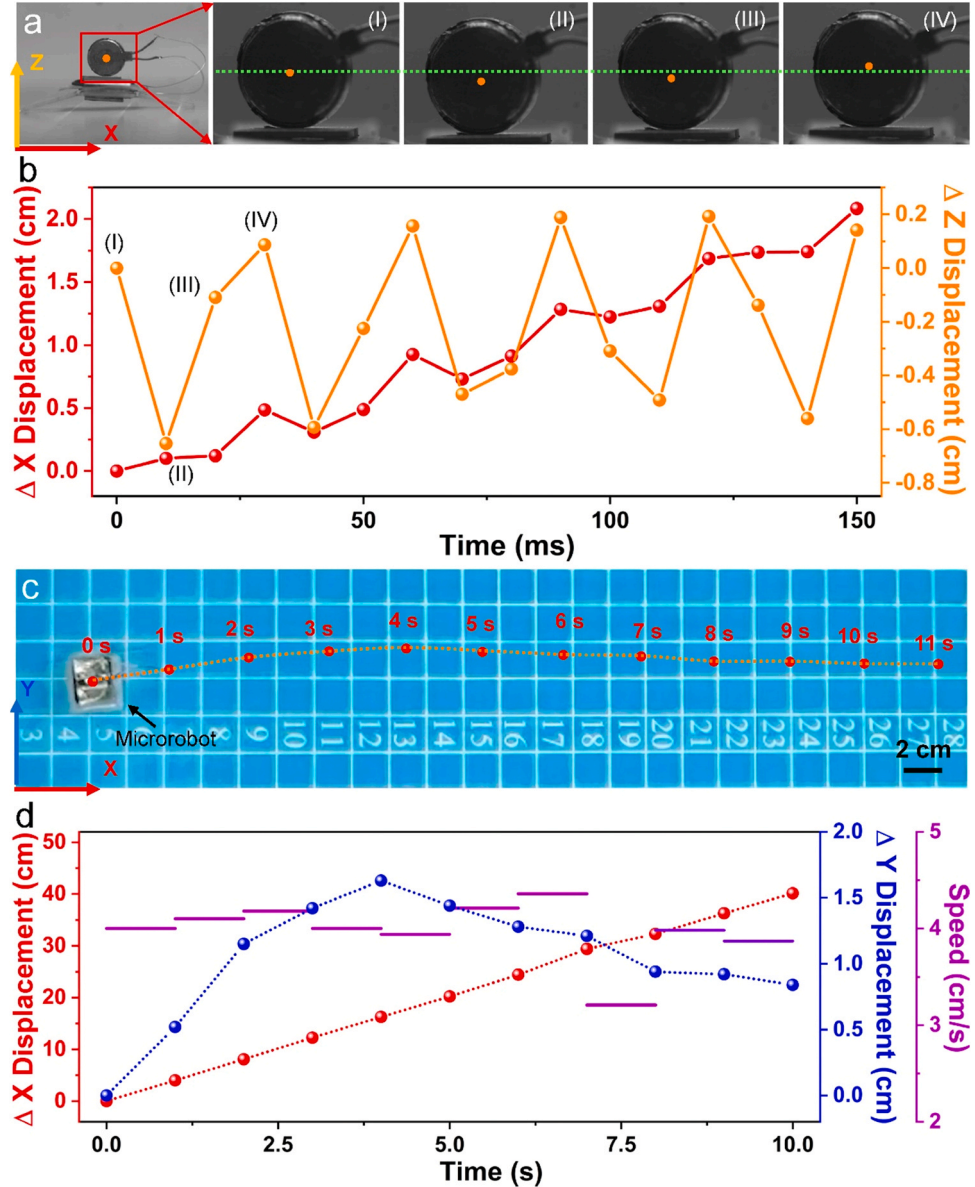


**Fig. 5.** Demonstration of microrobot locomotion. (a) Series of optical images showing the movements of the microrobot. (b) Vertical (yellow dots) and lateral displacements (red dots) of the microrobot. (c) Composite image of the microrobot moving on paper. The red dots represent the center of the microrobot at a given time. (d) Corresponding movement displacements and average speed analysis relative to time.

forward. Flexures are used instead of revolute joints to realize flexible bending deformation. The center of the robot has three main postures during movement: original posture, downward motion, and upward motion (Fig. 4b). In each state, the robot's body can be either expanding or retracting depending on the applied force from the motor and the supporting substrate. In this study,  $F$  is the vibration force, which generates pressure between the robot and substrate.  $F_1$  and  $F_2$  are the substrate reaction forces for the front and hind legs of the robot, respectively. Because the structure is asymmetric,  $F_2$  is greater than  $F_1$ , leading to forward locomotion of the robot.

We illustrate the locomotion mechanism of the robot using a dynamic mass-spring model (Fig. 4c) [52,55]. In this illustration, the torsional spring-damper system ( $k_\theta$ - $d_\theta$ ) represents the mechanical motions of the flexure. The vertical spring-damper ( $k$ - $d$ ) represents the ground contact, which consists of a normal force ( $F_N$ ) and a friction force ( $F_F$ ). The normal force is defined as [52]:

$$F_{nN} = \text{sign}(-y_{FN})\text{sign}(-ky_{FN} - dy_{FN})(-ky_{FN} - dy_{FN}) \quad (2)$$

where  $y_{FN}$  represents the position of the force;  $N = 1$  indicates the front leg and  $N = 2$  indicates the rear part of the robot. The normal force is considered as a spring-damper system ( $k$ - $d$ ) and the vertical force is positive. The motor is the driving source and generates other reaction forces. The higher effective spring constant of the cantilever stiffness for the hind leg results in a larger reaction force than that of the fore leg, leading to a forward force to achieve forward locomotion of the robot. Finite element method simulations were conducted to illustrate the stress distribution of the robot during movement. Most of the robot body is subjected to large pressure during the downward motion. The pressure gradually decreases during the restoration motion (Fig. 4d).

To locate the positions, we used a high-speed camera to track the robot COM. In the visual analysis of movement, we consider the center of the motor as the oscillatory COM to monitor the robot's motion trajectory. For the one cycle of motor vibration, the corresponding postures are illustrated as states (I) to (IV) (Fig. 5a). In state (I), the body is in the original posture. Thereafter, it spreads out, and the center reduces as a result of the vibration of the motor (state (II)). In state (III), the

restoration force from the supporting substrate lifts the center, leading to the upward movement of the robot. In state (IV), the center is at its highest position. These changes in the shape and the center position, and the asymmetric force acting on the robot body cause quick forward movement of the robot. Fig. 5b illustrates the lateral displacement (red dot) and vertical displacement (yellow dot) of the COM of the robot powered by the moisture-based energy harvesting device. The vertical displacement shows clear undulation and the lateral position of the COM shows incremental forward movement.

We further evaluated the stability of the forward movement of the microrobot. Fig. 5c shows a composite image of the robot moving on the paper where the red dot represents the COM of the robot (Movie S6). On the basis of the scaling relation between the lattice and the dots, we obtained the horizontal and longitudinal displacements. Fig. 5d shows that the robot can stably move on paper, with a slight deviation. The robot can maintain a stable speed of  $\sim 4.01$  cm/s during forward movement.

Supplementary material related to this article can be found online at doi:10.1016/j.nanoen.2021.106499.

Our work shows that moisture-based energy harvesting device can be embedded in the insect-scale robots to provide power. This design makes it possible to use the surrounding environment as a power source. We implemented a hygroscopic gel into the safe and established magnesium-based MAB chemistry, and enhanced the corresponding output voltage and current by using a cathode made of porous Cu foam decorated with  $\text{Co}_3\text{O}_4$  nanowires (Fig. S10). The device can operate in various environments and its output current increases with increasing RH. Our work could expand applications of current moisture-based energy harvesting devices [49,50].

Existing microrobots need LIBs or require an external stimulus. In contrast, our robot harvests energy from ambient humidity, with advantages of harmless and flexibility. For practical applications, our robot can operate at a low voltage of  $\sim 1.2$  V, making it suitable for further integration with low-power devices. Our robot does not perform controlled movement because it lacks an onboard system. To enable remote control, future research will incorporate sensors for position feedback. Furthermore, the power density and stability of the moisture-based energy harvesting devices will be further improved.

#### 4. Conclusion

In summary, we demonstrated an untethered self-powered micro-robot that can move without an external power source. The coupling of hygroscopic gel and oxygen reduction reaction enabled the microrobot to harvest energy from environment humidity. The moisture-based energy harvesting device is embedded into the robot body as a power unit. The integration of moisture-electricity powered vertical vibration and asymmetric structural design resulting in the forward movement of the microrobot. This work paves a way for the development of self-powered robots for environmental monitoring and exploration.

#### CRediT authorship contribution statement

W. C., Z. L.W. and Y. Y. supervised the research and conceived the idea. Y.W., and M.D. fabricated the composite materials. Y.W., M.D., H. W., L.X., and T.Z. carried out the device fabrication and the performance measurement. Y.W., M.D., W.C., Z.L.W., and Y.Y. analyzed the data and co-wrote the manuscript. All authors read and revised the manuscript.

#### Declaration of Competing Interest

The authors declare that they have no known competing financial interests or personal relationships that could have appeared to influence the work reported in this paper.

#### Acknowledgments

This work was supported by the National Key R&D Program of China (No. 2016YFA0202701), the National Natural Science Foundation of China (No. 52072041, 31922056), the University of Chinese Academy of Sciences (No. Y8540XX2D2) and Qingdao National Laboratory for Marine Science and Technology (No. 2017ASKJ01).

#### Appendix A. Supporting information

Supplementary data associated with this article can be found in the online version at doi:10.1016/j.nanoen.2021.106499.

#### References

- [1] R.J. Wood, The first takeoff of a biologically inspired at-scale robotic insect, *IEEE Trans. Robot* 24 (2008) 341–347.
- [2] W. Hu, G.Z. Lum, M. Mastrangeli, M. Sitti, Small-scale soft-bodied robot with multimodal locomotion, *Nature* 554 (2018) 81–85.
- [3] G.-Z. Yang, J. Bellingham, P.E. Dupont, P. Fischer, L. Floridi, R. Full, N. Jacobstein, V. Kumar, M. McNutt, R. Merrifield, B.J. Nelson, B. Scassellati, M. Taddeo, R. Taylor, M. Veloso, Z.L. Wang, R. Wood, The grand challenges of science robotics, *Sci. Robot* 3 (2018) eaar7650.
- [4] L. Hines, K. Petersen, G.Z. Lum, M. Sitti, Soft actuators for small-scale robotics, *Adv. Mater.* 29 (2017), 1603483.
- [5] G. Gu, J. Zou, R. Zhao, X. Zhao, X. Zhu, Soft wall-climbing robots, *Sci. Robot* 3 (2018) eaat2874.
- [6] Y. Chen, N. Doshi, B. Goldberg, H. Wang, R.J. Wood, Controllable water surface to underwater transition through electrowetting in a hybrid terrestrial-aquatic microrobot, *Nat. Commun.* 9 (2018) 2495.
- [7] H. Wang, Y. Liang, W. Gao, R. Dong, C. Wang, Emulsion hydrogel soft motor actuated by thermal stimulation, *ACS Appl. Mater. Interfaces* 9 (2017) 43211–43219.
- [8] W. Lai, C.K. Erdonmez, T.F. Marinis, C.K. Bjune, N.J. Dudney, F. Xu, R. Wartena, Y.-M. Chiang, Ultrahigh-energy-density microbatteries enabled by new electrode architecture and micropackaging design, *Adv. Mater.* 22 (2010) E139–E144.
- [9] Y.S. Song, M. Sitti, Surface-tension-driven biologically inspired water strider robots: theory and experiments, *IEEE Trans. Robot* 23 (2007) 578–589.
- [10] D.G. Mackanic, M. Kao, Z. Bao, Enabling deformable and stretchable batteries, *Adv. Energy Mater.* 10 (2020), 2001424.
- [11] T. Wang, C. Li, X. Xie, B. Lu, Z. He, S. Liang, J. Zhou, Anode materials for aqueous zinc ion batteries: mechanisms, properties, and perspectives, *ACS Nano* 14 (2020) 16321–16347.
- [12] K.Y. Ma, P. Chirattananon, S.B. Fuller, R.J. Wood, Controlled flight of a biologically inspired, insect-scale robot, *Science* 340 (2013) 603–607.
- [13] J.-S. Koh, E. Yang, G.-P. Jung, S.-P. Jung, J.H. Son, S.-I. Lee, P.G. Jablonski, R. J. Wood, H.-Y. Kim, K.-J. Cho, Jumping on water: surface tension-dominated jumping of water striders and robotic insects, *Science* 349 (2015) 517–521.
- [14] X. Zhang, J. Zhao, Q. Zhu, N. Chen, M. Zhang, Q. Pan, Bioinspired aquatic microrobot capable of walking on water surface like a water strider, *ACS Appl. Mater. Interfaces* 3 (2011) 2630–2636.
- [15] N.W. Bartlett, M.T. Tolley, J.T.B. Overvelde, J.C. Weaver, B. Mosadegh, K. Bertoldi, G.M. Whitesides, R.J. Wood, SOFT ROBOTICS: A 3D-printed, functionally graded soft robot powered by combustion, *Science* 349 (2015) 161–165.
- [16] T. Ranzani, S. Russo, N.W. Bartlett, M. Wehner, R.J. Wood, Increasing the dimensionality of soft microstructures through injection-induced self-folding, *Adv. Mater.* 30 (2018), 1802739.
- [17] Z. Ren, W. Hu, X. Dong, M. Sitti, Multi-functional soft-bodied jellyfish-like swimming, *Nat. Commun.* 10 (2019) 2703.
- [18] Y. Tang, Y. Chi, J. Sun, T.-H. Huang, O.H. Maghsoudi, A. Spence, J. Zhao, H. Su, J. Yin, Leveraging elastic instabilities for amplified performance: spine-inspired high-speed and high-force soft robots, *Sci. Adv.* 6 (2020) 6912.
- [19] S.-J. Park, M. Gazzola, K.S. Park, S. Park, V. Di Santo, E.L. Blevins, J.U. Lind, P. H. Campbell, S. Dauth, A.K. Capulli, F.S. Pasqualini, S. Ahn, A. Cho, H. Yuan, B. M. Maoz, R. Vijaykumar, J.-W. Choi, K. Deisseroth, G.V. Lauder, L. Mahadevan, K. Parker, Phototactic guidance of a tissue-engineered soft-robotic ray, *Science* 353 (2016) 158–162.
- [20] J. Mu, C. Hou, H. Wang, Y. Li, Q. Zhang, M. Zhu, Origami-inspired active graphene-based paper for programmable instant self-folding walking devices, *Sci. Adv.* 1 (2015), 1500533.
- [21] H. Lu, M. Zhang, Y. Yang, Q. Huang, T. Fukuda, Z. Wang, Y. Shen, A bioinspired multilegged soft millirobot that functions in both dry and wet conditions, *Nat. Commun.* 9 (2018) 3944.
- [22] J. Li, R. Zhang, L. Mou, M. Jung de Andrade, X. Hu, K. Yu, J. Sun, T. Jia, Y. Dou, H. Chen, S. Fang, D. Qian, Z. Liu, Photothermal Bimorph Actuators with In-Built Cooler for Light Mills, Frequency Switches, and Soft Robots, *Adv. Funct. Mater.* 29 (2019), 1808995.
- [23] A.S. Kuenstler, H. Kim, R.C. Hayward, Liquid crystal elastomer waveguide actuators, *Adv. Mater.* 31 (2019), 1901216.
- [24] Y. Wang, Y. Jiang, H. Wu, Y. Yang, Floating robotic insects to obtain electric energy from water surface for realizing some self-powered functions, *Nano Energy* 63 (2019), 103810.

- [25] P. Yang, K. Liu, Q. Chen, J. Li, J. Duan, G. Xue, Z. Xu, W. Xie, J. Zhou, Solar-driven simultaneous steam production and electricity generation from salinity, *Energy Environ. Sci.* 10 (2017) 1923–1927.
- [26] X. Chen, D. Goodnight, Z. Gao, A.H. Cavusoglu, N. Sabharwal, M. DeLay, A. Driks, O. Sahin, Scaling up nanoscale water-driven energy conversion into evaporation-driven engines and generators, *Nat. Commun.* 6 (2015) 7346.
- [27] X. Chen, L. Mahadevan, A. Driks, O. Sahin, Bacillus spores as building blocks for stimuli-responsive materials and nanogenerators, *Nat. Nanotechnol.* 9 (2014) 137–141.
- [28] A.-H. Cavusoglu, X. Chen, P. Gentine, O. Sahin, Potential for natural evaporation as a reliable renewable energy resource, *Nat. Commun.* 8 (2017) 617.
- [29] L. Cao, Q. Wen, Y. Feng, D. Ji, H. Li, N. Li, L. Jiang, W. Guo, On the origin of ion selectivity in ultrathin nanopores: insights for membrane-scale osmotic energy conversion, *Adv. Funct. Mater.* 28 (2018), 1804189.
- [30] F. Zhao, Y. Liang, H. Cheng, L. Jiang, L. Qu, Highly efficient moisture-enabled electricity generation from graphene oxide frameworks, *Energy Environ. Sci.* 9 (2016) 912–916.
- [31] B. Chen, X. Zhao, Y. Yang, Superelastic graphene nanocomposite for high cycle-stability water capture–release under sunlight, *ACS Appl. Mater. Interface* 11 (2019) 15616–15622.
- [32] H. Kim, S. Yang, S.R. Rao, S. Narayanan, E.A. Kapustin, H. Furukawa, A.S. Umans, O.M. Yaghi, E.N. Wang, Water harvesting from air with metal-organic frameworks powered by natural sunlight, *Science* 356 (2017) 430–434.
- [33] F. Fathieh, M.J. Kalmutzki, E.A. Kapustin, P.J. Waller, J. Yang, O.M. Yaghi, Practical water production from desert air, *Sci. Adv.* 4 (2018) 3198.
- [34] H. Kim, S.R. Rao, E.A. Kapustin, L. Zhao, S. Yang, O.M. Yaghi, E.N. Wang, Adsorption-based atmospheric water harvesting device for arid climates, *Nat. Commun.* 9 (2018) 1191.
- [35] N. Hanikel, M.S. Prévôt, O.M. Yaghi, MOF water harvesters, *Nat. Nanotechnol.* 15 (2020) 348–355.
- [36] Y. Guo, J. Bae, Z. Fang, P. Li, F. Zhao, G. Yu, Hydrogels and hydrogel-derived materials for energy and water sustainability, *Chem. Rev.* 120 (2020) 7642–7707.
- [37] A. LaPotin, Y. Zhong, L. Zhang, L. Zhao, A. Leroy, H. Kim, S.R. Rao, E.N. Wang, Dual-stage atmospheric water harvesting device for scalable solar-driven water production, *Joule* 5 (2021) 166–182.
- [38] G. Yilmaz, F.L. Meng, W. Lu, J. Abed, C.K.N. Peh, M. Gao, E.H. Sargent, G.W. Ho, Autonomous atmospheric water seeping MOF matrix, *Sci. Adv.* 6 (2020) eabc8605.
- [39] D.K. Nandakumar, Y. Zhang, S.K. Ravi, N. Guo, C. Zhang, S.C. Tan, Solar energy triggered clean water harvesting from humid air existing above sea surface enabled by a hydrogel with ultrahigh hygroscopicity, *Adv. Mater.* 31 (2019), 1806730.
- [40] J. Yang, X. Zhang, H. Qu, Z.G. Yu, Y. Zhang, T.J. Eey, Y.-W. Zhang, S.C. Tan, A moisture-hungry copper complex harvesting air moisture for potable water and autonomous urban agriculture, *Adv. Mater.* 32 (2020), 2002936.
- [41] M. Wang, T. Sun, D. Wan, M. Dai, S. Ling, J. Wang, Y. Liu, Y. Fang, S. Xu, J. Yeo, H. Yu, S. Liu, Q. Wang, J. Li, Y. Yang, Z. Fan, W. Chen, Solar-powered nanostructured biopolymer hygroscopic aerogels for atmospheric water harvesting, *Nano Energy* 80 (2021), 105569.
- [42] L. Zhu, T. Ding, M. Gao, C.K.N. Peh, G.W. Ho, Shape conformal and thermal insulative organic solar absorber sponge for photothermal water evaporation and thermoelectric power generation, *Adv. Energy Mater.* 9 (2019), 1900250.
- [43] D.K. Nandakumar, S.K. Ravi, Y. Zhang, N. Guo, C. Zhang, S.C. Tan, A super hygroscopic hydrogel for harnessing ambient humidity for energy conservation and harvesting, *Energy Environ. Sci.* 11 (2018) 2179–2187.
- [44] D.K. Nandakumar, J.V. Vaghasiya, L. Yang, Y. Zhang, S.C. Tan, A solar cell that breathes in moisture for energy generation, *Nano Energy* 68 (2020), 104263.
- [45] Y. Zhang, D.K. Nandakumar, S.C. Tan, Digestion of ambient humidity for energy generation, *Joule* 4 (2020) 2532–2536.
- [46] T. Xu, X. Ding, Y. Huang, C. Shao, L. Song, X. Gao, Z. Zhang, L. Qu, An efficient polymer moist-electric generator, *Energy Environ. Sci.* 12 (2019) 972–978.
- [47] F. Zhao, X. Zhou, Y. Liu, Y. Shi, Y. Dai, G. Yu, Super moisture-absorbent gels for all-weather atmospheric water harvesting, *Adv. Mater.* 31 (2019), 1806446.
- [48] L. Yang, S.K. Ravi, D.K. Nandakumar, F.I. Alzakia, W. Lu, Y. Zhang, J. Yang, Q. Zhang, X. Zhang, S.C. Tan, A hybrid artificial photocatalysis system splits atmospheric water for simultaneous dehumidification and power generation, *Adv. Mater.* 31 (2019), 1902963.
- [49] X. Liu, H. Gao, J.E. Ward, X. Liu, B. Yin, T. Fu, J. Chen, D.R. Lovley, J. Yao, Power generation from ambient humidity using protein nanowires, *Nature* 578 (2020) 550–554.
- [50] Y. Huang, H. Cheng, C. Yang, P. Zhang, Q. Liao, H. Yao, G. Shi, L. Qu, Interface-mediated hydroelectric generator with an output voltage approaching 1.5 volts, *Nat. Commun.* 9 (2018) 4166.
- [51] M.H. Dickinson, C.T. Farley, R.J. Full, M.A.R. Koehl, R. Kram, S. Lehman, How animals move: an integrative view, *Science* 288 (2000) 100–106.
- [52] Y. Wu, J.K. Yim, J. Liang, Z. Shao, M. Qi, J. Zhong, Z. Luo, X. Yan, M. Zhang, X. Wang, R.S. Fearing, R.J. Full, L. Lin, Insect-scale fast moving and ultrarobust soft robot, *Sci. Robot.* 4 (2019) eaax1594.
- [53] Y. Jiang, Y.-P. Deng, R. Liang, J. Fu, D. Luo, G. Liu, J. Li, Z. Zhang, Y. Hu, Z. Chen, Multidimensional ordered bifunctional air electrode enables fast reactants shuttling for high-energy flexible Zn-Air batteries, *Adv. Energy Mater.* 9 (2019), 1900911.
- [54] L. Peng, L. Shang, T. Zhang, G.I.N. Waterhouse, Recent advances in the development of single-atom catalysts for oxygen electrocatalysis and zinc-air batteries, *Adv. Energy Mater.* 10 (2020), 2003018.
- [55] H. Lu, Y. Hong, Y. Yang, Z. Yang, Y. Shen, Battery-less soft millirobot that can move, sense, and communicate remotely by coupling the magnetic and piezoelectric effects, *Adv. Sci.* 7 (2020), 2000069.
- [56] W. Chen, Q. Li, Y. Wang, X. Yi, J. Zeng, H. Yu, Y. Liu, J. Li, Comparative study of aerogels obtained from differently prepared nanocellulose fibers, *ChemSusChem* 7 (2014) 154–161.



**Yang Wang** is currently a postdoc fellow in Beijing Institute of Nanoenergy and Nanosystems, Chinese Academy of Sciences. He received his master's degree in Microelectronics Science and technology from Harbin University of Science and Technology, and Ph.D. degree in Electronics Science and Technology from Harbin Institute of Technology, China. His research currently focuses on self-powered sensors and bionic robot.



**Ming Dai** is a graduate student in the research group of Prof. Wenshuai Chen at Northeast Forestry University, China. She obtained her B.S. degree in Light Chemical Engineering from Northeast Forestry University in 2017. Her current research interests focus on the fabrication of functional nanostructured gels using wood cellulose nanofibers for air dehumidification.



**Heting Wu** is currently a postdoc fellow in Beijing Institute of Nanoenergy and Nanosystems, Chinese Academy of Sciences. She received her master's degree in University of Chinese Academy of Sciences. Her research currently focuses on electrochemical cells, triboelectric nanogenerators and there biomedical applications.



**Lin Xu** is a postgraduate of the School of Physics and Engineering Technology of Guangxi University. He is a currently visiting student at Beijing Institute of Nanoenergy and Nanosystems (BINN), Chinese Academy of Sciences. His main research is focused on organic composite materials and implantable robot.



**Tongtong Zhang** is a Ph.D. student in the research group of Professor Ya Yang at Beijing Institute of Nanoenergy and Nanosystems, Chinese Academy of Sciences (CAS). She received her bachelor's degree in Chemical Engineering and Technology from Guangxi University in 2018. Her current interests focus on self-powered sensors.



**Wenshuai Chen** is a professor in the College of Material Science and Engineering at Northeast Forestry University. He received his B.S. degree (2008) and Ph.D. degree (2013) in wood science and technology from Northeast Forestry University. His research interests include wood physics, bio-nanocomposites, nanocellulose, aerogels, and development of wood-based nanomaterials for energy and environmental sciences.



**Prof. Zhong Lin Wang** received his Ph.D. from Arizona State University in physics. He now is the Hightower Chair in Materials Science and Engineering, Regents' Professor, Engineering Distinguished Professor and Director, Center for Nanostructure Characterization, at Georgia Tech. Dr. Wang has made original and innovative contributions to the synthesis, discovery, characterization and understanding of fundamental physical properties of oxide nanobelts and nanowires, as well as applications of nanowires in energy sciences, electronics, optoelectronics and biological science. His discovery and breakthroughs in developing nanogenerators established the principle and technological road map for harvesting mechanical energy from environment and biological systems for powering a personal electronics. His research on self-powered nanosystems has inspired the worldwide effort in academia and industry for studying energy for micro-nano-systems, which is now a distinct disciplinary in energy research and future sensor networks. He coined and pioneered the field of piezotronics and piezophotonics by introducing piezoelectric potential gated charge transport process in fabricating new electronic and optoelectronic devices. Details can be found at: <http://www.nanoscience.gatech.edu>.



**Prof. Ya Yang** received his Ph.D. in Materials Science and Engineering from University of Science and Technology Beijing, China. He is currently a professor at Beijing Institute of Nanoenergy and Nanosystems, Chinese Academy of Sciences, China. He has developed ferroelectric materials-based various new hybridized and multi-effects coupled devices, opening up the new principles of the device design and coupled effects, and the new approaches of improving output performances of energy-related devices. His main research interests focus on the field of ferroelectric materials for energy conversion, self-powered sensing, and some new physical effects. Details can be found at: <http://www.researcherid.com/rid/A-7219-2016>.